Joule

CellPress

Article

Interfacial electrochemical-chemical reaction coupling for efficient olefin oxidation to glycols

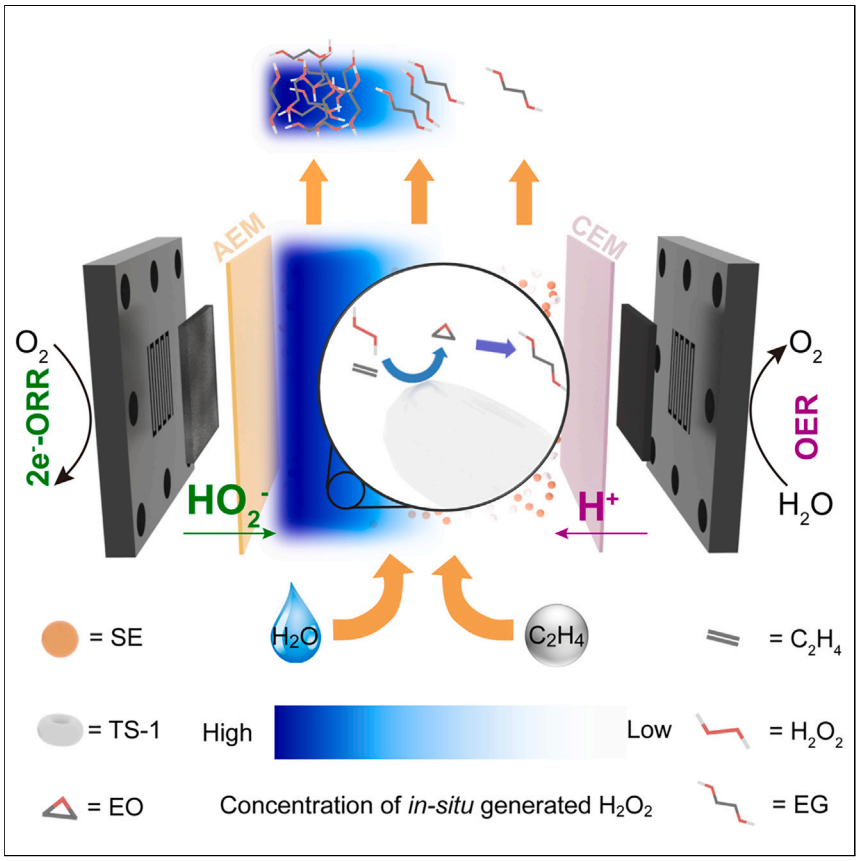

Using electrochemical reactions for chemical manufacturing can decarbonize our traditional chemical engineering industry. Although not every chemical can be generated via electrocatalysis, coupling electrochemical reactions with chemical reactions can significantly expand the spectrum of chemicals that can be produced in a low-carbon footprint manner. Here, we demonstrate an integrated electrochemical-chemical reactor that can efficiently produce ethylene glycol, which is an antifreeze and is widely used in the manufacture of polyester fibers, from oxygen and ethylene under room temperature and ambient pressure.

Shou-Kun Zhang, Yuge Feng, Ahmad Elgazzar, ..., Zachary Adler, Chase Sellers, Haotian Wang

htwang@rice.edu

Highlights

The demonstration of high interfacial H_2O_2 from electrolysis

Interfacial effect boosted olefin epoxidation with a 3-fold increase over a tandem system

Potential application for boosting reactant concentration-sensitive reactions

Electrolyte-free liquid products from electrolysis

Zhang et al., Joule 7, 1–15
August 16, 2023
https://doi.org/10.1016/j.joule.2023.06.022

Please cite this article in press as: Zhang et al., Interfacial electrochemical-chemical reaction coupling for efficient olefin oxidation to glycols, Joule (2023), https://doi.org/10.1016/j.joule.2023.06.022

Joule

CellPress

Article

Interfacial electrochemical-chemical reaction coupling for efficient olefin oxidation to glycols

Shou-Kun Zhang,[1] Yuge Feng,[1] Ahmad Elgazzar,[1] Yang Xia,[1] Chang Qiu,[1] Zachary Adler,[1] Chase Sellers,[1] and Haotian Wang[1,2,3,4,*]

SUMMARY

Coupling electrochemical and chemical reactions has been demonstrated in traditional tandem reactor systems, but their practical applications are still distilled down to individual reactor optimizations. Here, we demonstrate a fully integrated system that presents significantly improved catalytic performance when compared with traditional tandem systems. Using electrosynthesis of hydrogen peroxide followed by olefin epoxidation reaction as a representative example, we demonstrated that, by confining the chemical reaction right at the electrode/electrolyte interface in our solid electrolyte reactor, we can fully leverage the interfacial high concentration of H_2O_2 product from electrocatalysis to boost the following ethylene epoxidation reaction, which represented a 3-fold improvement in electrolyte-free ethylene glycol generation when compared with a tandem reactor system. This integration strategy can be extended to other electrochemical-chemical coupling reactions, especially when the coupled reaction is sensitive to reactant concentrations, which could avoid energy-intensive separation or concentration steps typically needed between the electrochemical and chemical reactions.

CONTEXT & SCALE

Electrochemical synthesis of chemicals and fuels plays an important role in decarbonizing the chemical manufacturing sector due to the merits of using renewable electricity, mild reaction conditions, and environmentally benign operations. Despite the significant achievements of individual electrochemical reactions, coupling electrolyzers with downstream reactors is increasingly attractive from more complicated chemical fabrications that are typically challenging for individual reactors. Current coupling reactions focus on the assembly strategies of multiple individual reactors by feeding the electrochemically synthesized species into the followed-by reactors, which have not yet leveraged the unique property of electrolysis: the high concentration of generated species at the electrode interface. Different from the traditional tandem system, we designed an integrated solid electrolyzer that fully leverages the interfacial high concentration of species to boost the consecutive chemical reactions.

INTRODUCTION

Electrochemical synthesis of chemicals and fuels is becoming increasingly important to decarbonize the chemical manufacturing sector.[1–8] It can utilize renewable electricity as the energy input, be operated under mild reaction conditions, and use atmospheric molecules as reactants.[9–13] As the economics of electrochemical synthesis routes gradually improve with the decreased renewable electricity price and further technological development, the chemical industry will witness more and more electrolyzers playing significant roles along industrial supply chains.[14–16]

Although the technological improvements and device scaling-up of individual electrochemical reactions, such as water splitting and CO_2 reduction,[17–20] remain the focal points in the field, we have begun to see more recent reports on coupling electrochemical reactors with upstream or downstream reactors for more complicated products that are typically impossible from electrolyzers alone.[21–26] One typical coupling strategy is the tandem system, where the electrochemically generated intermediate products are continuously fed into a downstream reactor for product upgradation (Figure 1A). Examples include coupling electrochemical devices with bioreactors for the conversion of CO_2 into high-value chemicals (Figure 1A).[27–29] Another type of coupling is the mediator coupling reaction, in which the anodically or cathodically generated reaction mediators, such as Cl^- to ClO^- or Cl radicals, as

Please cite this article in press as: Zhang et al., Interfacial electrochemical-chemical reaction coupling for efficient olefin oxidation to glycols, Joule (2023), https://doi.org/10.1016/j.joule.2023.06.022

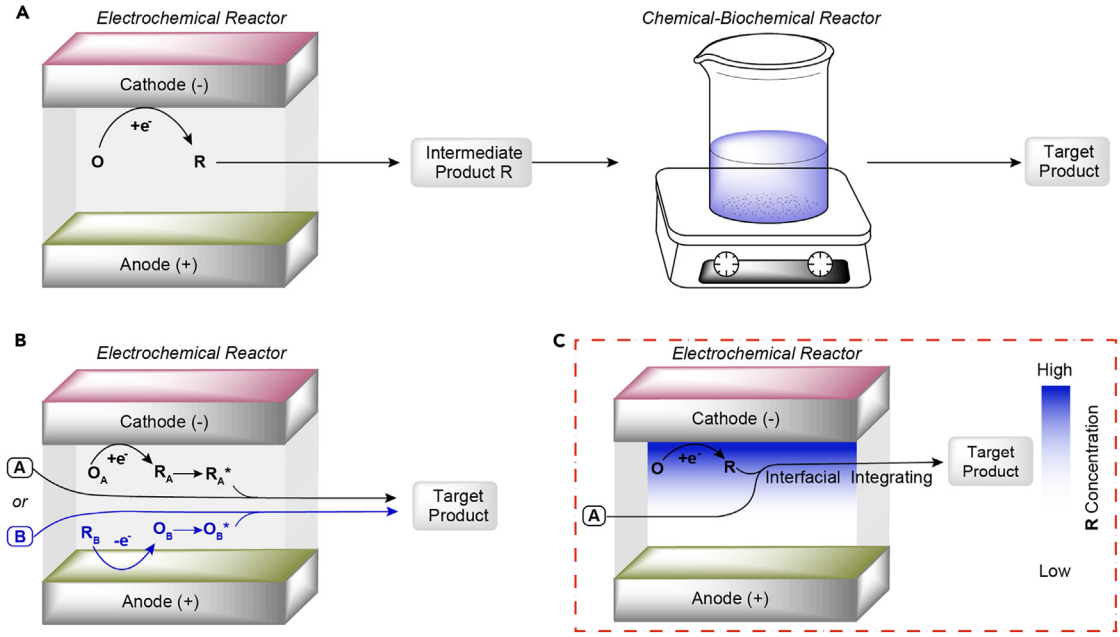

Figure 1. Different reactor coupling strategies

(A) Traditional tandem reaction where electrochemically generated intermediate products are continuously fed into a downstream reactor for product upgradation.

(B) Mediator coupling reactions by using the mediator produced at the cathode or anode.

(C) Ideal system: integrated electrochemical-chemical reaction coupling strategy by efficiently using the electrogenerated highly concentrated interfacial intermediates for subsequent reactions.

well as O_2 to •OH, can homogeneously react with a fed-in reactant for obtaining the target product and are converted back to their original status for the next round of reaction (Figure 1B).[30–34]

Although exciting progress has been made in the development of these coupling reactions, their design and engineering are still distilled down to individual reaction optimizations, which have not yet leveraged one unique property of electrocatalysis: the high concentration of generated products/intermediates at the catalyst/electrolyte interface.[35,36] As is well documented in electrocatalysis, the surface-generated molecules are typically accumulated at the catalyst/electrolyte interface before they slowly diffuse away into the bulk electrolyte or the gas chamber. For example, in the formation of liquid products, due to the sharp catalyst/electrolyte interface (typically in micrometer scales) compared with bulk electrolyte (typically in millimeter scales), the product concentration at this interfacial region could be orders of magnitude higher than the average concentration when all the molecules are well dispersed into the electrolyte.[37] However, in a traditional electrochemical-chemical tandem reaction system, this concentration gradient will disappear before the product stream flows into the downstream reactor, losing the opportunity to make full use of the high interfacial concentrations to accelerate the follow-up reaction. How to leverage this unique property in electrocatalysis and the impacts of this interfacial high concentration on the follow-up reaction activity are still unclear.[38]

Different from traditional coupling systems, here, we demonstrated an interfacial electrochemical-chemical reaction coupling design to fully leverage the interfacial high product concentrations in electrochemistry to boost the consecutive chemical reactions (Figure 1C). Using olefin epoxidation reaction as a model reaction, which

[1]Department of Chemical and Biomolecular Engineering, Rice University, Houston, TX, USA

[2]Department of Materials Science and NanoEngineering, Rice University, Houston, TX, USA

[3]Department of Chemistry, Rice University, Houston, TX, USA

[4]Lead contact

*Correspondence: htwang@rice.edu

https://doi.org/10.1016/j.joule.2023.06.022

Please cite this article in press as: Zhang et al., Interfacial electrochemical-chemical reaction coupling for efficient olefin oxidation to glycols, Joule (2023), https://doi.org/10.1016/j.joule.2023.06.022

is sensitive to the concentration of oxidants,[39] we integrated oxygen reduction reaction (ORR) to hydrogen peroxide (H_2O_2) with a subsequent ethylene (C_2H_4) epoxidation reaction (to ethylene glycol [EG]) into one solid electrolyte (SE) reactor. This integration allowed us to achieve a 3-fold improvement in EG production rates and 2-fold in H_2O_2 utilization efficiencies when compared with a traditional tandem reactor system. Specifically, by directly feeding ethylene into the SE layer of our integrated reactor, under a 25 mA/cm^2 ORR current density, the EG production rate can reach 583 μmol/h, delivering a H_2O_2 utilization efficiency of 96% and an overall Faradaic efficiency of 98.7%. This interfacial reaction integration strategy can be extended to other electrochemical-chemical coupling reactions, especially when the coupled chemical reaction is sensitive to reactant concentrations.

Concept demonstration

Glycols, especially EG and propylene glycol (PG), are important feedstocks for industrial polymer synthesis and antifreezes, which are normally obtained from the direct oxidation of olefins[40] or hydrolysis of olefin oxides.[41,42] Recently, using H_2O_2 instead of chlorine for olefin epoxidation on titanium silicalite-1 (TS-1) catalyst, especially the well-known hydrogen peroxide to propylene oxidation (HPPO) process,[43] has attracted extensive attention in both industry and academia due to its high product selectivity and environmentally benign process (producing H_2O as the byproduct).[44–48] In our group's recent studies on the electrochemical synthesis of H_2O_2, we developed a unique SE reactor that enables direct and continuous synthesis of high purity H_2O_2 solutions via 2e$^-$–ORR.[49–51] By performing 2e$^-$–ORR electrolysis on the cathode, H_2O_2 molecules could be continuously formed at the membrane/SE interface via ionic recombination between HO_2^- (transported from the cathode) and H^+ (transported from the anode). When mixing TS-1 catalyst particles inside the middle SE layer, this integrated SE reactor can serve as a perfect platform to demonstrate the interfacial electrochemical-chemical reaction coupling strategy—we can leverage the high local concentration of H_2O_2 molecules to boost the following olefin epoxidation reaction before they gradually diffuse and are diluted into the bulk deionized (DI) water stream.

In order to prove this concept, we designed a novel three-chamber SE reactor to realize an interfacial integration of electrochemical and chemical reactions (Figures 2 and S1). The main chamber (middle layer) of the SE cell was filled with a mixture of SE and TS-1 particles and was separated by an anion exchange membrane (AEM) and cation exchange membrane (CEM) from the cathode and anode, respectively. The cathodic ORR via 2e$^-$–ORR catalyst (carbon black) could selectively generate HO_2^- species that were subsequently transported through AEM into the middle layer (Figure 2B, Equation 1). These anion species were recombined with the proton flux that was transported from the anode chamber via the CEM and SE particles (proton conductors) (Figure 2B, Equations 2 and 3). Therefore, the AEM/SE interface has the highest H_2O_2 concentration during electrolysis. By co-feeding ethylene and DI water into the middle chamber during ORR electrolysis, ethylene can be efficiently oxidized by the interfacial H_2O_2 to generate ethylene oxide (EO) (Figure 2B, Equation 4), followed by the hydrolysis on the surface of SE to form EG as the final product (Figures 2B, Equation 5 and S2; Notes S1 and S2). Combined with half-cell oxygen evolution reaction (OER) at the anode (Figure 2B, Equation 2) and the coupled chemical epoxidation reaction in the main chamber (Figure 2B, Equations 3–5), we can conclude the overall reaction using O_2, ethylene, and DI water as reactants and EG as the only product with an excellent atom economy (Figure 2B, Equation 6).

Please cite this article in press as: Zhang et al., Interfacial electrochemical-chemical reaction coupling for efficient olefin oxidation to glycols, Joule (2023), https://doi.org/10.1016/j.joule.2023.06.022

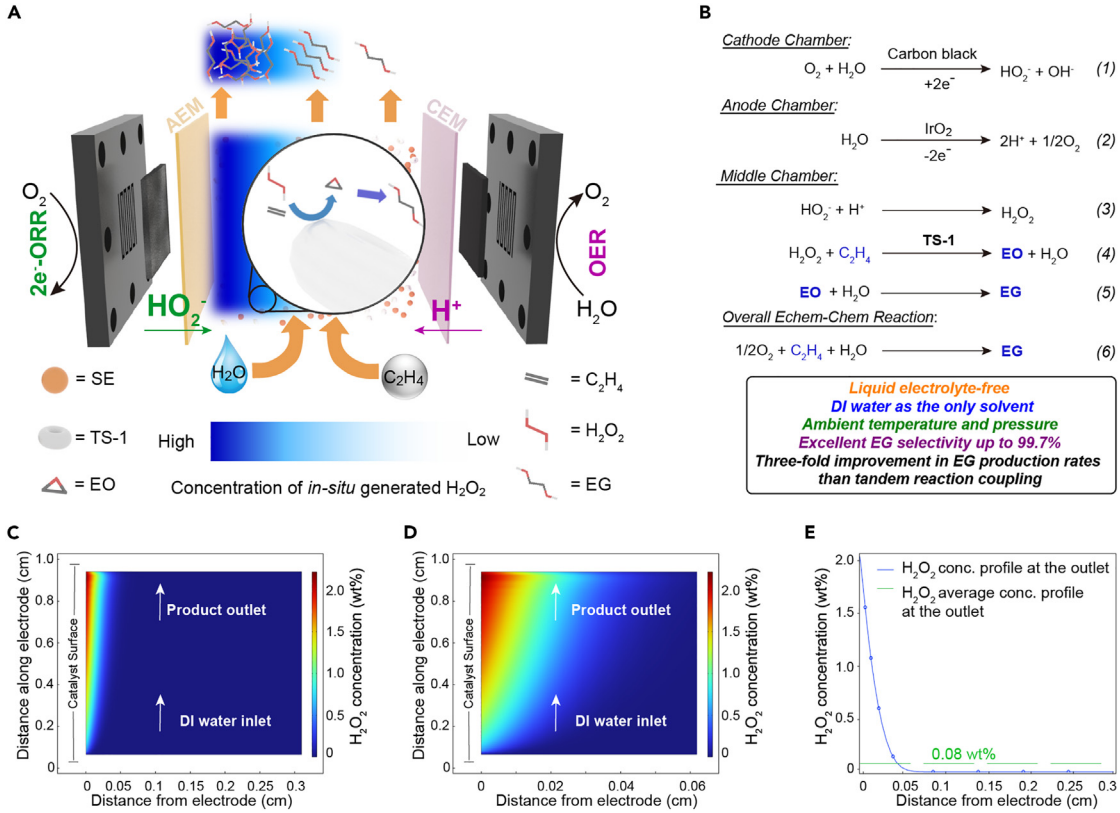

Figure 2. Our integrated solid electrolyte reactor design for interfacial electrochemical-chemical reaction coupling

(A) Schematic of our integrated three-chamber solid electrolyte (SE) reactor. See also Figure S1.

(B) Proposed reaction mechanism.[39] See also Figure S2.

(C and D) COMSOL modeling for H_2O_2 distribution in the middle SE layer under a 25 mA/cm^2 2e$^-$–ORR current. See also Figure S3.

(E) Comparison between the interfacial concentration and the average concentration of generated H_2O_2 at the outlet of the middle layer.

To have a rough understanding of how high the interfacial H_2O_2 concentration could be in our SE reactor when compared with the downstream output concentration (average bulk concentration), we constructed a two-dimensional (2D) COMSOL model to map out the H_2O_2 concentration distribution near the catalyst surface (Figures 2C–2E and S3). As expected, the H_2O_2 concentration is highest at the left-hand boundary, where the reaction occurs and H_2O_2 flux is introduced. The H_2O_2 concentration reaches above 2.06 wt % closer to the surface at 25 mA/cm^2, whereas the average concentration in the channel is around 0.081 wt % (Figure 2C). This results in an interfacial concentration that is more than 25 times higher than the average concentration in the channel. This simulation result suggests that, if we can confine the following epoxidation reaction right at the catalyst/electrolyte interface, the overall efficiency of the coupling reaction could be dramatically boosted.

RESULTS AND DISCUSSION

Because commercial TS-1 catalyst is not ionically conductive, we need to balance mass loading of the catalyst and the SE within the middle layer to guarantee a low ohmic loss while maximizing the epoxidation reaction rate (which is correlated with the TS-1 loading). Similar particle sizes of SE and TS-1 catalyst were chosen to ensure a uniform distribution during the continuous water flow (Figures S4–S5; Note S3). We first fixed a 1:1 mass ratio of SE to TS-1 in our reactor to investigate the impact of TS-1 catalysts on the catalytic performance of the integrated SE reactor

Please cite this article in press as: Zhang et al., Interfacial electrochemical-chemical reaction coupling for efficient olefin oxidation to glycols, Joule (2023), https://doi.org/10.1016/j.joule.2023.06.022

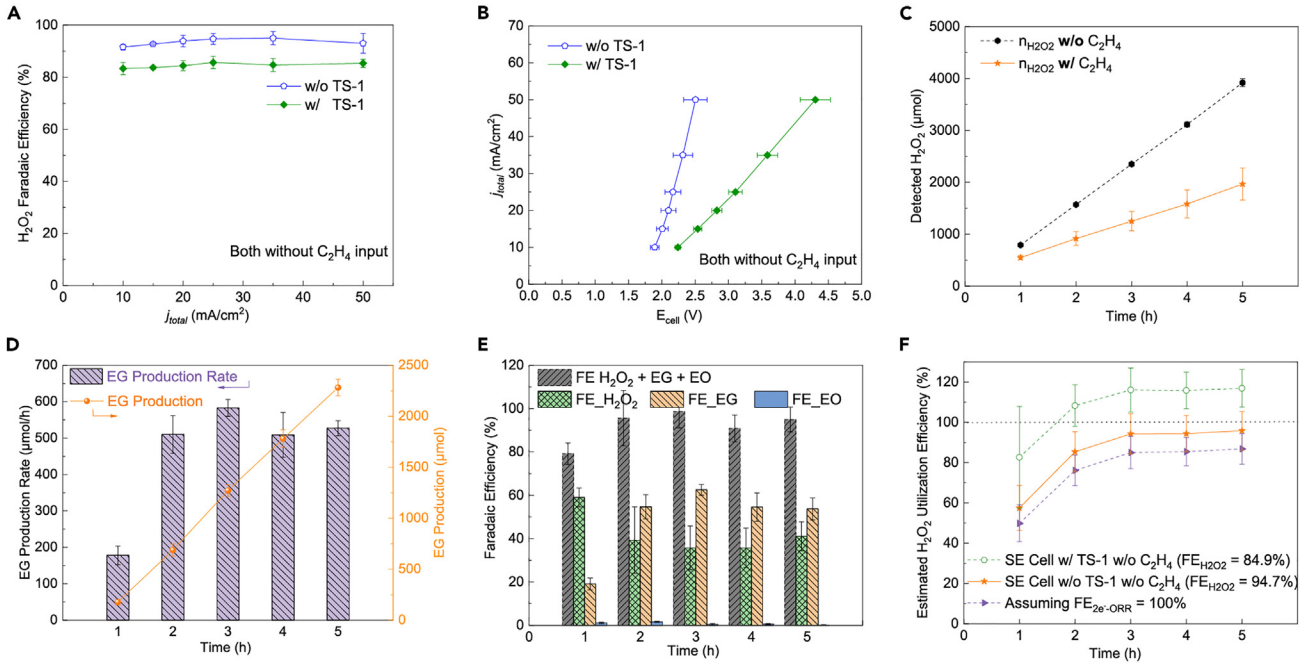

Figure 3. Catalyst characterization and cell performance at a fixed ORR current of j_{total} = 25 mA/cm^2

Without further notification, the standard reaction conditions are as follows: 2 cm^2 electrode area (1.38 cm × 1.45 cm), 20 mL DI water (0.70 mL/min recirculation flowrate) and 1 mL/min C_2H_4 flow, 1:1 ratio of TS-1 to SE (by weight, the total middle layer loading is 740 mg) in the middle chamber (2.5 cm × 2.5 cm × 0.25 cm), and continuous electrolysis time of 5 h. Target products were analyzed in an average value after a corresponding reaction period. Measurements were taken at least three times, and the average values are listed with the standard deviation as error bars. The H_2O_2 production, EG production, EG selectivity, and H_2O_2 utilization efficiency were analyzed in an accumulative way (over the whole reaction period), whereas the EG production rate and the Faradaic efficiency were analyzed instantaneously during the past 1-h period if there was no further notification. See also Figures S4–S12.

(A and B) The Faradaic efficiencies of H_2O_2 and IV curves at various applied current densities without C_2H_4 input of the SE reactor with (green) and without (blue) TS-1 catalyst inside the middle layer chamber.

(C) H_2O_2 accumulation of our integrated SE reactor (cell assembled with TS-1 catalysts) with (orange) or without (black) C_2H_4 input.

(D) Accumulation (orange) and instantaneous production rate (purple) of EG.

(E) Faradaic efficiencies of remaining H_2O_2 (green), generated EG (purple), and EO (blue), and the sum of them (gray), representing the FE of 2e$^-$–ORR.

(F) Three types of methods for evaluating H_2O_2 utilization efficiency, assuming FE_{H2O2} = 100% (purple); FE_{H2O2} = 94.7% (H_2O_2 performance in the SE reactor without TS-1 catalyst, orange); FE_{H2O2} = 84.9% (H_2O_2 performance in the SE reactor with TS-1 catalyst, green).

(without introducing ethylene). As shown in Figures 3A and 3B, the introduction of TS-1 only slightly decreased the Faradaic efficiencies of H_2O_2 from 92%–94% to 83%–86% and increased the cell voltage from 1.89–2.50 V to 2.24–4.31 V, which may be due to accelerated H_2O_2 self-decomposition on TS-1 catalyst and increased middle layer resistance, respectively (Figure S6; Note S4). To precisely quantify the generated H_2O_2 and EG and accumulate a baseline H_2O_2 concentration, we continuously recirculated a certain volume of DI water through the middle layer of our reactor (see experimental procedures and schematic Figure S7). Under a fixed ORR current of 25 mA/cm^2 without ethylene, the H_2O_2 concentration showed almost linear increase to a bulk concentration of 0.67 wt % during the 5-h electrolysis (Figure S8), with an average production rate of 784 μmol/h (Figure 3C). This accumulated H_2O_2 concentration sharply decreased when ethylene was introduced to the middle layer, suggesting the utilization of H_2O_2. By analyzing the recirculated DI water using nuclear magnetic resonance (NMR) spectroscopy, we were able to detect the generation of both EG and EO, with EG being the dominant species (>95%, Figures S9 and S10). No other side products, such as glycolaldehyde, acetaldehyde, or formic acid, were detected (Figures S10–S12).[40] The production rate of EG gradually increased from 178 μmol/h at the first hour to a steady state of over 500 μmol/h (Figure 3D).

Please cite this article in press as: Zhang et al., Interfacial electrochemical-chemical reaction coupling for efficient olefin oxidation to glycols, Joule (2023), https://doi.org/10.1016/j.joule.2023.06.022

One possible reason for this improved performance was that the H_2O_2 bulk concentration gradually increased from 0 to 0.33 wt % (Figure S8). A more likely reason could be the TS-1 catalyst activation process as reported by Copéret et al.,[39] where the TS-1 catalyst was activated by consuming *in situ*-generated H_2O_2 to form the active catalytic species, resulting in less H_2O_2 than expected during the initial olefin epoxidation. Our experimental results also supported this hypothesis (Figure 3E). The overall Faradaic efficiency of detected ORR and epoxidation products, including EG, EO, and the remaining H_2O_2, was around 98.7% under steady-state reaction rates, which was close to the $2e^-$–ORR selectivity (~95%) in our SE reactor and suggested the full detection of all significant products. However, the overall Faradaic efficiency (FE) in the first hour was only 79%, missing an obvious portion that was consumed during the catalyst activation process. The maximal FE_{EG} we achieved was at ~63%, suggesting that 63% of the overall ORR electrons were eventually used for EG generation, and the corresponding FE_{H2O2} was at ~36%, which represents the part of H_2O_2 that was not used for epoxidation and was responsible for the continuous increase of H_2O_2 baseline concentration (Figure 3C). Another important parameter in this reactor system is the H_2O_2 utilization efficiency (Figure 3F; defined in experimental procedures), which is, however, not straightforward to measure precisely. There are three ways to evaluate the H_2O_2 utilization efficiency based on the estimation of total generated H_2O_2. First, the lower limit can be obtained by assuming a 100% intrinsic H_2O_2 FE, yielding up to 87% H_2O_2 utilization efficiency (Figure 3F, purple). Second, a more realistic estimation is to assume the $2e^-$–ORR intrinsic FE, when coupled with TS-1 and ethylene epoxidation, is similar to the intrinsic H_2O_2 FE of 94.7% in our SE reactor without TS-1 catalyst, resulting in up to 96% H_2O_2 utilization efficiency (Figure 3F, orange). The estimated utilization efficiency could surpass 100% (Figure 3F, green) if we use a detected H_2O_2 FE (85%) when TS-1 catalyst was introduced but without ethylene (Figure 3B, green), suggesting that the species generated during the TS-1 catalyst activation process could also be utilized for ethylene epoxidation. Thus, we decided to use the second method to describe our H_2O_2 utilization efficiency as the most realistic estimation in this study.

Analysis of the interfacial effect

To confirm the interfacial effects on EG generation in our integrated SE reactor, we prepared different concentrations of 20 mL H_2O_2 solution, ranging from 0.11 to 5.0 wt %, to be directly fed and recirculated into the middle chamber of our reactor together with ethylene but without ORR electrolysis. The concentrations from 0.11 to 0.6 wt % were prepared to roughly match the average H_2O_2 concentrations generated via $2e^-$–ORR (at ~85% H_2O_2 FE) at different reaction times (1, 2, 3, 4, and 5 h, respectively), assuming no H_2O_2 utilization. The aim of this control experiment was to examine the EG production performance under a uniformly distributed H_2O_2 electrolyte and compare it with that of interfacial integrated reaction. The results shown in Figures 4A and 4B suggest a profound impact of the interfacial reaction. In the case of 0.6 wt % H_2O_2 solutions, which is close to the average H_2O_2 concentration after a 5-h continuous $2e^-$–ORR electrolysis without consumption, the EG production was only 41% of that when coupling the ethylene oxidation with ORR at the interface (Figure 4A). The performance of bulk electrolyte reactions eventually caught up with the interfacial integrated reaction system when we used a 5.0 wt % H_2O_2 solution, suggesting a powerful interfacial effect. More importantly, the H_2O_2 utilization efficiency of our interfacial coupling system outperformed the case of uniform H_2O_2 concentration (Figure 4C), which guarantees a good balance of both high catalytic reaction rate and high H_2O_2 utilization efficiency for future practical applications (for more details, see Figure S13 and Note S5).

Please cite this article in press as: Zhang et al., Interfacial electrochemical-chemical reaction coupling for efficient olefin oxidation to glycols, Joule (2023), https://doi.org/10.1016/j.joule.2023.06.022

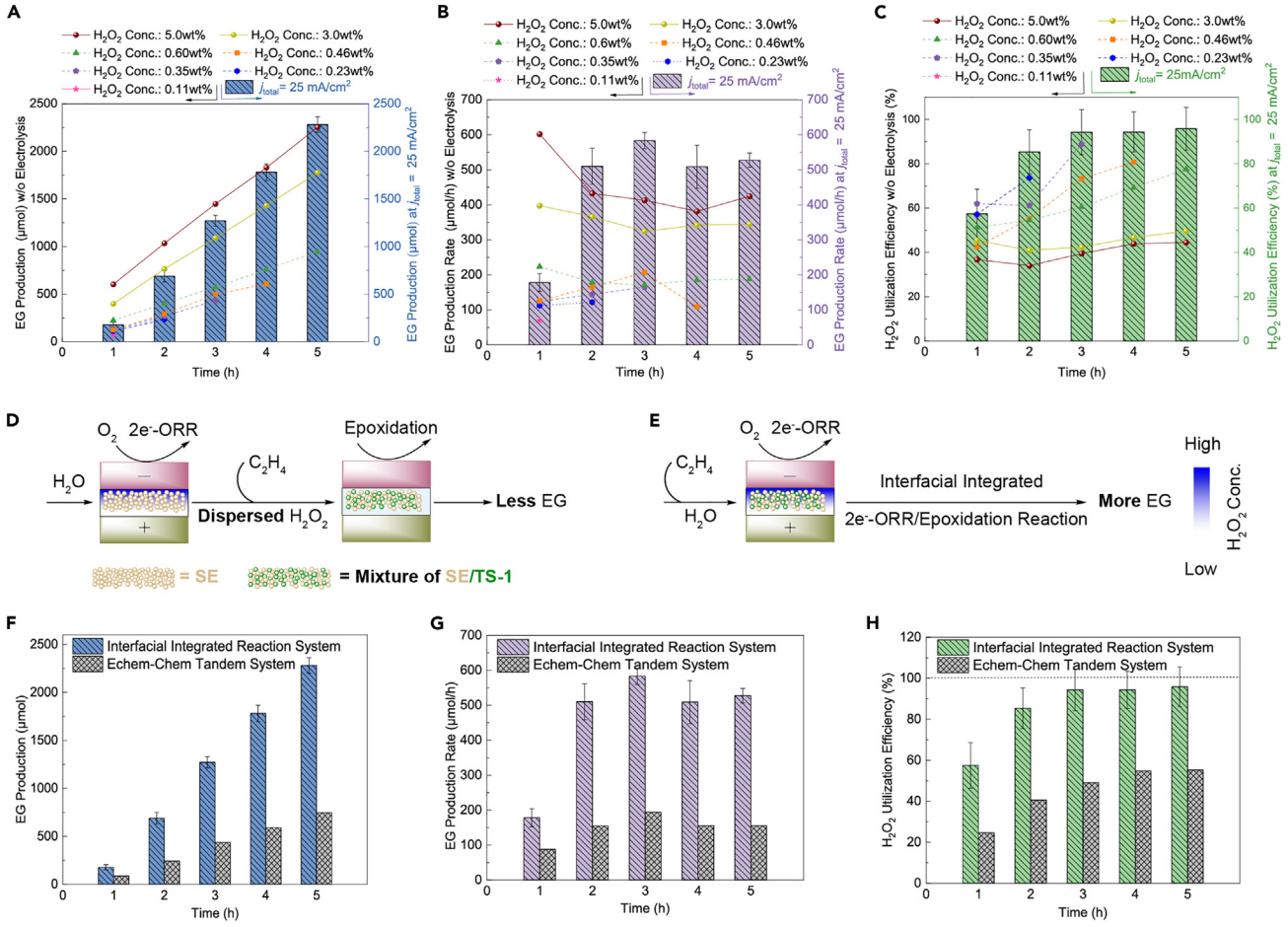

Figure 4. Comparison between the interfacial integrated reaction system and the traditional tandem reaction system

(A–C) The EG accumulation, production rate, and H_2O_2 utilization efficiency were measured by directly co-feeding different concentrations of H_2O_2 solutions with C_2H_4 into the SE/TS-1 middle layer without ORR electrolysis. Experimental results without error bars were averaged by at least two data points if there was no further notification. Without further notification, all the data from the 25 mA/cm^2 conditions stem from the same experiments, with Figure 3 for comparison. See also Figure S13.

(D and E) Schematics of a traditional tandem reaction system and our interfacial electrochemical-chemical reaction coupling system.

(F–H) The EG production comparison between our interfacial integrated SE reactor and the traditional Echem-Chem tandem reactor under an ORR current of j_{total} = 25 mA/cm^2. See also Figure S14.

To directly compare our interfacial integrated reaction system with the traditional tandem reaction system (Figures 4D and 4E), we evaluated the EG generation performance by separating the ORR to H_2O_2 and the C_2H_4 epoxidation reaction into two independent reactors—the first one is our regular SE reactor only for H_2O_2 generation without TS-1 catalyst or C_2H_4 input; the generated H_2O_2 stream and C_2H_4 were co-fed into the second reactor for epoxidation. Please note here that the second reactor, without electrolysis, is the same as our integrated SE reactor (TS-1 catalyst and SE particle mixture) for a fair epoxidation reaction comparison. After a 5-h electrolysis at 25 mA/cm^2, the EG accumulation and production rate (Figures 4F and 4G) from the electrochemical-chemical tandem reactor were only 1/3, and the H_2O_2 utilization efficiency (Figures 4H and S14; Note S6) was only half of those in our interfacial integrated electrochemical-chemical reactor, suggesting the great advantage of our interfacial electrochemical-chemical reaction coupling strategy over traditional tandem systems. As a side note, the EG production performance

Please cite this article in press as: Zhang et al., Interfacial electrochemical-chemical reaction coupling for efficient olefin oxidation to glycols, Joule (2023), https://doi.org/10.1016/j.joule.2023.06.022

of the tandem reactor was also in good agreement with that of direct H_2O_2 feeding without electrolysis. For example, the tandem reactor *via* a 4-h $2e^-$–ORR electrolysis generated 592 μmol of EG (Figure 4F), whereas the direct feeding of 0.46 wt % of H_2O_2, which is equivalent to the amount of H_2O_2 generated during the 4-h electrolysis, in total generated 607 μmol EG (Figure 4A).

Impacts of cation, ORR current density, and TS-1 loading on EG generation

Furthermore, a series of control experiments were performed for the optimization and improvement of our integrated SE reactor. Without considering the downstream separation of impurity ions, the introduction of liquid electrolytes (such as Na_2SO_4, NaH_2PO_4, and K_2HPO_4) instead of pure DI water could decrease the cell resistance and improve the cell voltages. However, regardless of whether their pH values were slightly acidic (NaH_2PO_4), neutral (Na_2SO_4), or slightly basic (K_2HPO_4), the liquid electrolytes all exhibited significantly lower performance on EG production (only 11%–28% of that with DI water flow) and lower H_2O_2 utilization efficiency (41%–65% vs. 96%) when comparing with DI water flow in SEs (Figures 5A–5D and S15). Although the presence of cations in the middle layer does not affect the FE of $2e^-$–ORR, we suspect that the epoxidation reaction rate could be negatively affected by alkaline cations, suggesting the important role of proton flux or the SE's acidic sites for the epoxidation reaction (Note S7).[52–54]

The EG generation performance of our integrated system is relevant to both the H_2O_2 generation rate and the epoxidation reaction rate, which act synergistically. Therefore, different current densities ranging from 10 to 50 mA/cm^2 were tested to understand the impact of H_2O_2 generation rates. In Figures 5E and S16, the EG production was observed to be linearly scaled with the applied current densities in the range of 10 to 25 mA/cm^2. However, when we further increased the current to 50 mA/cm^2, the increase in EG production started to deviate from the linear increase. This observation suggested that, in the current cell configuration, the overall reaction rate was limited by H_2O_2 generation before 25 mA/cm^2 and was limited by the epoxidation reaction when the ORR current was higher than 25 mA/cm^2 (for more details, see Figure S16C and Note S8). We must emphasize here that the epoxidation reaction in our system has not been optimized yet and there is still lot of room to improve it, including by enhancing the mass transport of C_2H_4 gas to the reaction sites and the surface area and porosity of TS-1 catalyst. The impact of TS-1 catalyst loading was also analyzed. As expected, the decrease in catalyst loading resulted in decreased EG generation rate, Faradaic efficiency, selectivity, and H_2O_2 utilization efficiency (Figures 5I–5L and S17). More catalyst loading, especially at the AEM/SE interface, could further improve our EG production in the future.

Long-term stability test

The long-term stability of our interfacial electrochemical/chemical reaction coupling system was evaluated under a fixed ORR current (10 mA/cm^2) in 200 mL of recirculated DI water (Figures 6A–6D and S18–S19). The cell potential during the 200-h electrolysis gradually increased from ~2 to ~4 V, probably due to membrane degradation and the continuous accumulation of organic products (EG) (Figure 6A; Note S9). From the production rate of EG, it was clear that catalyst pre-activation required around 20 h when using a lower current density and a larger volume of recirculated solution, yielding a relatively diluted H_2O_2 bulk concentration (Figure 6B; Note S10). Our interfacial reaction coupling system could accumulate EG with an excellent selectivity of 99.7% to 150 mM (with a volume of 200 mL DI water) in 200 h and a high H_2O_2 utilization efficiency of 93% (Figures 6C and 6D). A thinner AEM (for more details, see Figure S19 and Note S11) was also used for stability test and

Please cite this article in press as: Zhang et al., Interfacial electrochemical-chemical reaction coupling for efficient olefin oxidation to glycols, Joule (2023), https://doi.org/10.1016/j.joule.2023.06.022

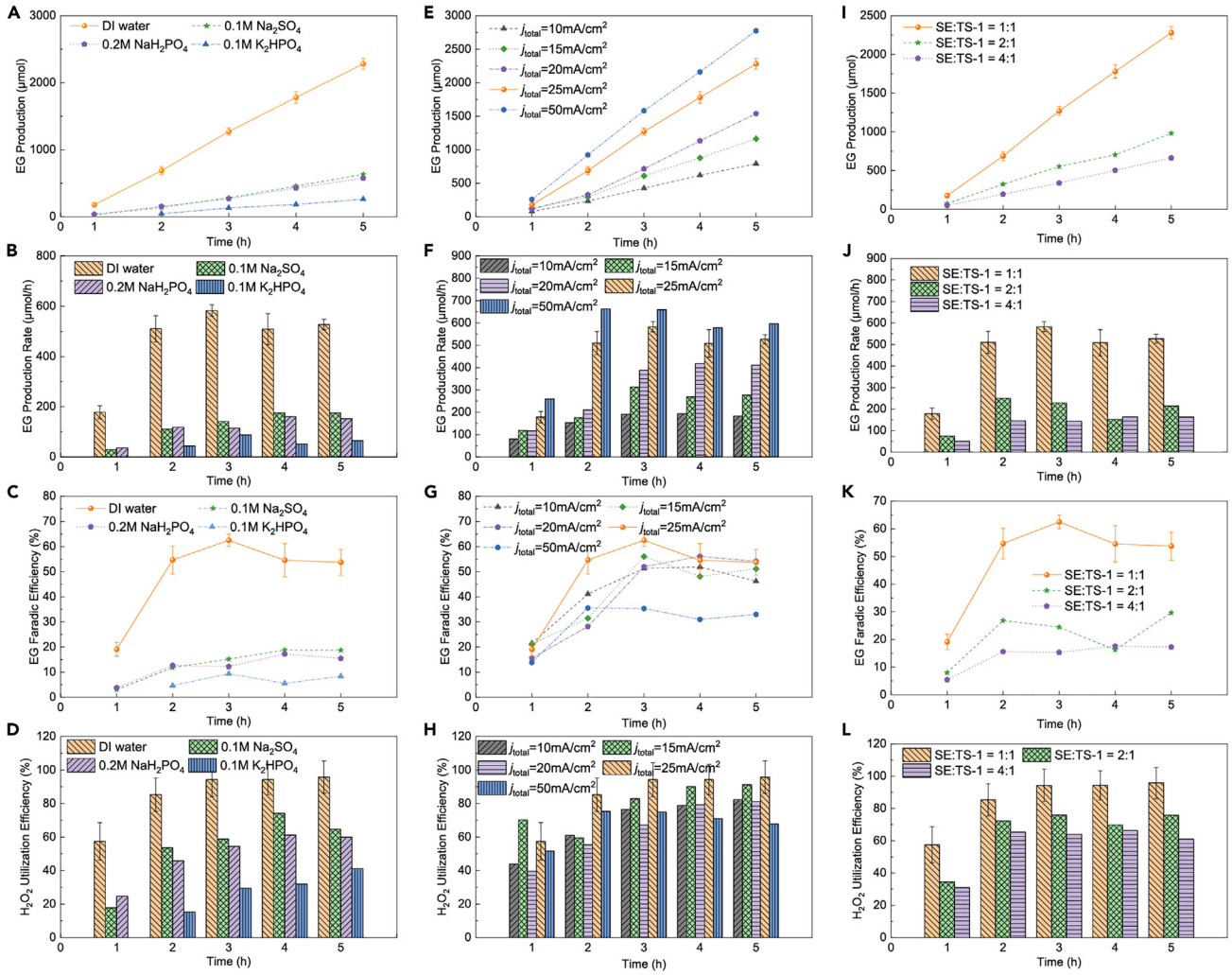

Figure 5. The EG production analysis under different liquid electrolytes, current densities, and TS-1 catalyst loadings

EG production, EG production rate, EG Faradaic efficiency, and H_2O_2 utilization efficiency were compared under the following:

(A–D) Different liquid electrolyte (j_{total} = 25 mA/cm^2): DI water (orange), 0.1M Na_2SO_4 (green), 0.2M NaH_2PO_4 (purple), and 0.1M K_2HPO_4 (blue).

(E–H) Different current densities (10–50 mA/cm^2).

(I–L) Different TS-1 catalyst loading (j_{total} = 25 mA/cm^2): SE:TS-1 = 1:1 (TS-1: ~370 mg, orange), SE:TS-1 = 2:1 (TS-1: ~246 mg, green), SE:TS-1 = 4:1 (TS-1: ~148 mg, purple). See also Figures S15–S17.

gave a slightly higher EG Faradaic efficiency of 70% (53% from the thicker AEM), demonstrating the robustness of our integrated electrochemical-chemical SE reactor for utilizing the interfacial species.

Conclusions

In summary, we designed an integrated electrochemical-chemical reaction coupling reactor, which demonstrated superior performance and design advantages when compared with traditional tandem coupling reactions. To achieve this exceptional capability, our integrated three-chamber SE reactor efficiently utilizes the electrochemical *in situ*-generated highly concentrated intermediates at the cathode interface for the desired chemical reaction. By paring the 2e$^-$–ORR electrolysis with a model olefin epoxidation, our integrated reactor demonstrated an over 300% increase in EG formation and a 175% higher H_2O_2 utilization efficiency compared with the typical tandem

Please cite this article in press as: Zhang et al., Interfacial electrochemical-chemical reaction coupling for efficient olefin oxidation to glycols, Joule (2023), https://doi.org/10.1016/j.joule.2023.06.022

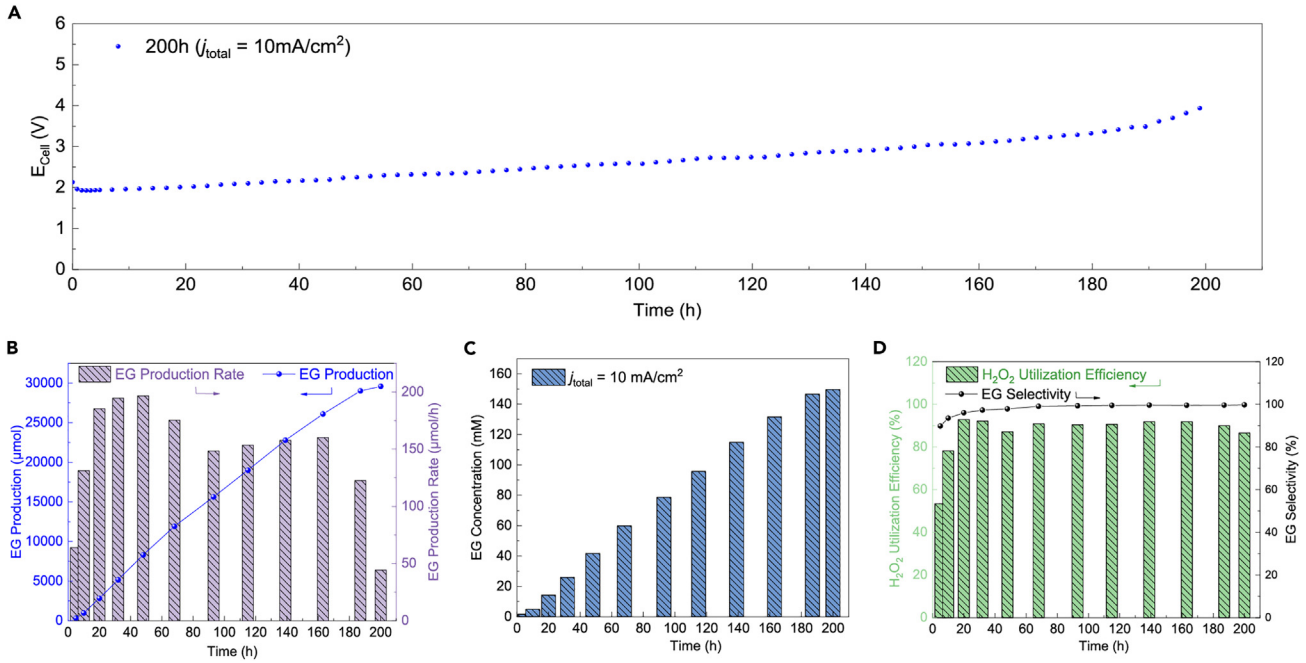

Figure 6. Stability testing

Standard condition variation: using a Sustainion® X37–50 Grade T (~82 um thickness), 200 mL DI water, and j_{total} =10 mA/cm^2.

(A) Cell potential over 200 h continuous operation under 10 mA/cm^2.

(B) EG production rate (purple column) and accumulated EG generation (blue line).

(C) Accumulated concentration of EG.

(D) Utilization efficiency of H_2O_2 (green column) and selectivity of EG (black line). See also Figures S18–S19.

reactor. Moreover, without using any liquid electrolyte, our SE reactor achieved a 200-h operation to furnish pure EG with an excellent EG selectivity of 99.7% and H_2O_2 utilization efficiency of 93%, which avoided additional expense for further salt purification. With a current density of 25 mA/cm^2, our design could achieve an EG production rate of 583 μmol/h, along with a H_2O_2 utilization efficiency of 96%. Although the EG production rate could be improved to 663 μmol/h at 50 mA/cm^2, the real breakthrough would be seeking a more highly active material, and we are currently focusing on this critical area of investigation. Importantly, our integrated device is not only suitable for olefin epoxidation but also serves as a powerful framework to enhance other electrochemical reactions coupled with reactant concentration-sensitive chemical reactions, which could avoid energy-intensive separation or concentration steps typically needed between the electrochemical and chemical reactions.

EXPERIMENTAL PROCEDURES

Resource availability

Lead contact

Further information and requests for resources and materials should be directed to and will be fulfilled by the lead contact, Haotian Wang (htwang@rice.edu).

Materials availability

This study did not generate new unique materials.

Data and code availability

This study did not generate or analyze datasets or code.

Please cite this article in press as: Zhang et al., Interfacial electrochemical-chemical reaction coupling for efficient olefin oxidation to glycols, Joule (2023), https://doi.org/10.1016/j.joule.2023.06.022

Chemicals and materials

TS-1 was purchased from ACS Material. C_2H_4 (>99.9%) was purchased from Airgas. SE (Amberchrom 50WX8, 200–400 mesh, hydrogen form), NaH_2PO_4 (≥99.0%), K_2HPO_4 (≥99.0%), Na_2SO_4 (≥99.0%), MeCN (≥99.8%), H_2SO_4 (95.0%–98.0%), EG (>99.8%), EO (50 mg/mL in methanol), 0.1 N $KMnO_4$ standardized solution, Nafion 117 solution (5%), and isopropanol were all purchased from Sigma-Aldrich. D_2O (99.9% D) was purchased from Cambridge Isotope Laboratories. Sigracet 28 BC gas diffusion layer (GDL) and Nafion 1110 were purchased from Fuel Cell Store. Carbon black (BP2000) was purchased from Cabot Corporation. AEM (Sustainion X37–50 Grade T) and IrO_2 on carbon paper (OER catalyst) were purchased from dioxide materials.

ORR catalyst preparation

15 mg BP2000, 120 μL 5% Naffion 117, and 4 mL IPA were added to a 10 mL glass vial and sonicated for 1 h. Subsequently, this ink was sprayed onto a GDL (6 × 6 cm^2) via a spray gun. Finally, it was dried and cut into 1.38 × 1.45 cm^2 (density of ORR catalyst is around 0.41 mg/cm^2) species as cathode.

Epoxidation catalyst (TS-1) characterization

All X-ray diffraction (XRD) spectra were calibrated by shifting the detected carbon C 1s peak to 284.6 eV, and scanning electron microscope (SEM) spectra were performed on a FEI Quanta 400 field emission SEM.

Interfacial electrochemical-chemical reaction coupling reaction test

All the electrochemical measurements were performed at ambient temperature. A BioLogic VMP3 workstation was employed to record the electrochemical response without infrared (IR) compensation. GDL (2 cm^2) loaded with BP2000 was used as ORR catalyst, and commercial IrO_2 on GDL (2 cm^2) was used as OER catalyst. The three-chamber SE cell was composed of a cathode chamber, an anode chamber, and a middle layer filled with the mixture of SE and TS-1 (or only SE), which was separated by an AEM and a CEM. The cathode chamber was fed with an O_2 flow rate of 15 mL/min and the anode chamber was fed with a 0.20 mL/min DI water flow rate. 20 mL of DI water or 20 mL of certain concentrated H_2O_2 (electrochemically generated from our SE cell to eliminate the effect of stabilizer in the commercial H_2O_2) in a 20 mL glass vial was recycled with a 0.70 mL/min flow rate into the main chamber (middle layer) and then co-fed with C_2H_4 (gas flow rate: around 1 mL/min) through a Y-Type connector. After the desired reacting time, 40 μL of liquid was used for the titration of H_2O_2 and 50 μL for ^{1}H-NMR (500 or 600 MHz) or/and ^{13}C-NMR (151 MHz) to do the liquid product analysis (using 3 μmol of MeCN per 100 μL of D_2O solution as the internal standard). NMR spectra were recorded on a 500 or 600 MHz standard-bore (SB) Liquid Bruker Advance NMR spectrometer using water suppression technology.

H_2O_2 concentration was measured by standard potassium permanganate (0.1 N $KMnO_4$ solution, Sigma-Aldrich) titration process, according to following equation:

$$2KMnO_4 + 5H_2O_2 + 3H_2SO_4 \rightarrow 2MnSO_4 + K_2SO_4 + 5O_2 + 8H_2O$$

In this project, under certain conditions, 40–100 μL of liquid product was collected for $KMnO_4$ titration.

Preparing the internal standard solution

Solution **A**: (300 μmol/100 uL in D_2O): 783 μL MeCN into 5 mL volumetric flask, filled up with D_2O to 5 mL.

Internal standard solution **B**: (3 μmol/100 μL in D_2O): 1 mL solution **A** into a 100-mL volumetric flask, filled up with D_2O to 100 mL, and solution **B** was used for the NMR analysis. The volumes of certain reaction solutions (40–100 μL) and internal standards (40–100 μL) are mixed with a volume ratio of 1/1.

$$n_{EG} = \frac{S_{EG}/N_{EG}}{S_{CH3CN}/N_{CH3CN}} \times n_{CH3CN}$$

$$n_{EO} = \frac{S_{EO}/N_{EO}}{S_{CH3CN}/N_{CH3CN}} \times n_{CH3CN}$$

(n_{CH3CN} [mol], n_{EG} [mol], and n_{EO} [mol] are the amounts of added internal standard MeCN and generated products EG and EO; S_{EG} and S_{CH3CN} are the peak areas in ^{1}H-NMR spectra; N_{EG}, N_{EO}, and N_{CH3CN} are the number of protons in HOC_2H_4OH [N_{EG} = 4], C_2H_4O [N_{EO} = 4], and CH_3CN [N_{MeCN} = 3]).

The calculation of H_2O_2, EG, and EO Faradaic efficiency and EG selectivity and production rate

H_2O_2, EG, and EO Faradaic efficiency (FE_{H2O2}, FE_{EG}, and FE_{EO}):

$$FE_{H2O2}\ (\%) = \frac{Conc._{H2O2}\ (mol/L) \times Volume(L) \times 2 \times 96485(C/mol)}{j_{total}\ (mA) \times time(s)} \times 100.$$

$$FE_{EG}\ (\%) = \frac{Conc._{EG}\ (mol/L) \times Volume(L) \times 2 \times 96485(C/mol)}{j_{total}\ (mA) \times time(s)} \times 100.$$

$$FE_{EO}\ (\%) = \frac{Conc._{EO}\ (mol/L) \times Volume(L) \times 2 \times 96485(C/mol)}{j_{total}\ (mA) \times time(s)} \times 100.$$

($Conc._{H2O2}$ [mol/L], $Conc._{EG}$ [mol/L], and $Conc._{EO}$ [mol/L] are the concentrations of generated H_2O_2, EG, and EO).

Note: Theoretically, the epoxidation of olefin with H_2O_2 to form EO and the followed-up hydrolysis of EO into EG are not electrochemical reactions. To standardize the quantitative measurement of the interfacial integrated $2e^-$–ORR/epoxidation reaction, we have also employed an electrochemical quantitative method to calculate EO and EG Faradaic efficiencies. EO and EG were obtained from H_2O_2 and C_2H_4 via two-electron transfer.

EG selectivity:

$$\text{EG selectivity}\ (\%) = \frac{n_{EG}}{n_{EG}+n_{EO}} \times 100.$$

EG production rate:

$$\text{EG production rate}\ (\mu mol\,/\,h) = \frac{n_{EG}(t_2) - n_{EG}(t_1)}{t_2 - t_1} \times 100.$$

After a time of t_1 (h) and t_2 (h), EG was obtained with a value of $n_{EG}(t_1)$ (μmol) and $n_{EG}(t_2)$ (μmol).

Please cite this article in press as: Zhang et al., Interfacial electrochemical-chemical reaction coupling for efficient olefin oxidation to glycols, Joule (2023), https://doi.org/10.1016/j.joule.2023.06.022

Two methods for calculating the H_2O_2 utilization efficiency
Measurement for a $2e^-$–ORR/epoxidation reaction coupling.

$$H_2O_2 \text{ utilization efficiency } (\%) = \frac{n_{EG}+n_{EO}}{n^g_{H2O2} \times FE^{realistic}_{H2O2} - n^r_{H2O2}} \times 100.$$

(n^g_{H2O2}: generated H_2O_2 [mol] if FE_{H2O2} = 100%; $FE^{realistic}_{H2O2}$ = H_2O_2 Faradaic efficiency [94.7%, SE reactor without TS-1 nor C_2H_4], n^r_{H2O2}: remaining H_2O_2 [mol] after $2e^-$–ORR/epoxidation reaction).

Measurement for an epoxidation reaction when using different concentrated H_2O_2 concentration without electrolysis.

$$H_2O_2 \text{ utilization efficiency } (\%) = \frac{n_{EG}+n_{EO}}{n^s_{H2O2} - n^r_{H2O2}} \times 100.$$

(n^s_{H2O2}: starting amount of H_2O_2 [mol]; n^r_{H2O2}: remaining H_2O_2 [mol] after reaction).

Interfacial H_2O_2 concentration modeling

To achieve this, we utilized the transport of dilute species in porous media and single-phase flow modules to simulate the H_2O_2 flux at a current density of 25 mA/cm^2, a DI water flow rate of 0.7 mL/min through a SE with 0.45 porosity, and an H_2O_2 Faradaic efficiency of 95%. Due to the convection effects of the DI water flow, areas closer to the water inlet are more diluted than areas further up along the electrode surface (Figures 2C and 2D). It confirms the fully developed flow profile with no-slip boundary conditions on the side walls (Figure S3). As expected, the flow reaches its maximum at the center and gradually decreases as it approaches the static walls.

$\nabla.J_i + u.\nabla c_i = R_i + S_i$ is solved numerically by the model, which considers both diffusion and convection contributions. The velocity "u" required for this calculation is obtained by solving the Navier-Stokes equation. H_2O_2 production rate is calculated using $j_{H_2O_2} = \frac{FE_{H_2O_2} * j_{total}}{n*A*F}$ where $j_{H_2O_2}$ is the flux of H_2O_2, j_{total} is the applied current, n is the number of electrons transferred, A is the area, and F represents Faraday's constant.

SUPPLEMENTAL INFORMATION

Supplemental information can be found online at https://doi.org/10.1016/j.joule.2023.06.022.

ACKNOWLEDGMENTS

This work was supported by Shell (contract No. CW643915). We appreciate the suggestions and discussions with researchers from Shell: Reza Mirshekari, Sander van Bavel, Alexander Vander Made, and Oyinkansola Romiluyi, during the project.

AUTHOR CONTRIBUTIONS

S.-K.Z. and H.W. conceptualized the project. H.W. supervised the project. S.-K.Z. conducted the catalytic tests of catalysts and the related data processing. S.-K.Z. and H.W. wrote the manuscript. Y.F. designed the schematic. Y.F. and C.Q. performed the materials characterization. A.E. and Z.A. conducted the COMSOL modeling part. Y.X. and C.S. repeated the experiment. All authors discussed the results and commented on the manuscript.

DECLARATION OF INTERESTS

The authors declare no competing interests.

INCLUSION AND DIVERSITY

We support inclusive, diverse, and equitable conduct of research.

Received: April 21, 2023
Revised: June 15, 2023
Accepted: June 29, 2023
Published: July 24, 2023

REFERENCES

1. She, X., Wang, Y., Xu, H., Chi Edman Tsang, S., and Ping Lau, S.P. (2022). Challenges and opportunities in electrocatalytic CO_2 reduction to chemicals and fuels. Angew. Chem. Int. Ed. Engl. *61*, e202211396.
2. Meyer, T.H., Choi, I., Tian, C., and Ackermann, L. (2020). Powering the future: how can electrochemistry make a difference in organic synthesis? Chem *6*, 2484–2496.
3. Liu, J., Lu, L., Wood, D., and Lin, S. (2020). New redox strategies in organic synthesis by means of electrochemistry and photochemistry. ACS Cent. Sci. *6*, 1317–1340.
4. Anson, C.W., and Stahl, S.S. (2020). Mediated fuel cells: soluble redox mediators and their applications to electrochemical reduction of O_2 and oxidation of H_2, alcohols, biomass, and complex fuels. Chem. Rev. *120*, 3749–3786.
5. Wiebe, A., Gieshoff, T., Möhle, S., Rodrigo, E., Zirbes, M., and Waldvogel, S.R. (2018). Electrifying organic synthesis. Angew. Chem. Int. Ed. Engl. *57*, 5594–5619.
6. Tang, S., Liu, Y., and Lei, A. (2018). Electrochemical oxidative cross-coupling with hydrogen evolution: A green and sustainable way for bond formation. Chem *4*, 27–45.
7. Jiang, Y., Xu, K., and Zeng, C. (2018). Use of electrochemistry in the synthesis of heterocyclic structures. Chem. Rev. *118*, 4485–4540.
8. Yan, M., Kawamata, Y., and Baran, P.S. (2017). Synthetic organic electrochemical methods since 2000: on the verge of a renaissance. Chem. Rev. *117*, 13230–13319.
9. Zhao, X., Levell, Z.H., Yu, S., and Liu, Y. (2022). Atomistic understanding of two-dimensional electrocatalysts from first principles. Chem. Rev. *122*, 10675–10709.
10. Vogt, C., Monai, M., Kramer, G.J., and Weckhuysen, B.M. (2019). The renaissance of the Sabatier reaction and its applications on Earth and in space. Nat. Catal. *2*, 188–197.
11. Jouny, M., Hutchings, G.S., and Jiao, F. (2019). Carbon monoxide electroreduction as an emerging platform for carbon utilization. Nat. Catal. *2*, 1062–1070.
12. Birdja, Y.Y., Pérez-Gallent, E., Figueiredo, M.C., Göttle, A.J., Calle-Vallejo, F., and Koper, M.T.M. (2019). Advances and challenges in understanding the electrocatalytic conversion of carbon dioxide to fuels. Nat. Energy *4*, 732–745.
13. Chu, S., Cui, Y., and Liu, N. (2016). The path towards sustainable energy. Nat. Mater. *16*, 16–22.
14. Tang, C., Zheng, Y., Jaroniec, M., and Qiao, S.Z. (2021). Electrocatalytic refinery for sustainable production of fuels and chemicals. Angew. Chem. Int. Ed. Engl. *60*, 19572–19590.
15. Masel, R.I., Liu, Z., Yang, H., Kaczur, J.J., Carrillo, D., Ren, S., Salvatore, D., and Berlinguette, C.P. (2021). An industrial perspective on catalysts for low-temperature CO_2 electrolysis. Nat. Nanotechnol. *16*, 118–128.
16. Smith, W.A., Burdyny, T., Vermaas, D.A., and Geerlings, H. (2019). Pathways to industrial-scale fuel out of thin air from CO_2 electrolysis. Joule *3*, 1822–1834.
17. Yang, M., Zhang, C.H., Li, N.W., Luan, D., Yu, L., and Lou, X.W.D. (2022). Design and synthesis of hollow nanostructures for electrochemical water splitting. Adv. Sci. (Weinh) *9*, e2105135.
18. Cohen, K.Y., Evans, R., Dulovic, S., and Bocarsly, A.B. (2022). Using light and electrons to bend carbon dioxide: developing and understanding catalysts for CO_2 conversion to fuels and feedstocks. Acc. Chem. Res. *55*, 944–954.
19. Tackett, B.M., Gomez, E., and Chen, J.G. (2019). Net reduction of CO_2 via its thermocatalytic and electrocatalytic transformation reactions in standard and hybrid processes. Nat. Catal. *2*, 381–386.
20. Liu, Y., Xiao, C., Huang, P., Cheng, M., and Xie, Y. (2018). Regulating the charge and spin ordering of two-dimensional ultrathin solids for electrocatalytic water splitting. Chem *4*, 1263–1283.
21. Guan, X., Erşan, S., Hu, X., Atallah, T.L., Xie, Y., Lu, S., Cao, B., Sun, J., Wu, K., Huang, Y., et al. (2022). Maximizing light-driven CO_2 and N_2 fixation efficiency in quantum dot–bacteria hybrids. Nat. Catal. *5*, 1019–1029.
22. Su, Y., Cestellos-Blanco, S., Kim, J.M., Shen, Y.-x., Kong, Q., Lu, D., Liu, C., Zhang, H., Cao, Y., and Yang, P. (2020). Close-packed nanowire-bacteria hybrids for efficient solar-driven CO_2 fixation. Joule *4*, 800–811.
23. Cestellos-Blanco, S., Zhang, H., Kim, J.M., Shen, Y.-x., and Yang, P. (2020). Photosynthetic semiconductor biohybrids for solar-driven biocatalysis. Nat. Catal. *3*, 245–255.
24. Haas, T., Krause, R., Weber, R., Demler, M., and Schmid, G. (2018). Technical photosynthesis involving CO_2 electrolysis and fermentation. Nat. Catal. *1*, 32–39.
25. Guo, J., Suástegui, M., Sakimoto, K.K., Moody, V.M., Xiao, G., Nocera, D.G., and Joshi, N.S. (2018). Light-driven fine chemical production in yeast biohybrids. Science *362*, 813–816.
26. Li, H., Opgenorth, P.H., Wernick, D.G., Rogers, S., Wu, T.Y., Higashide, W., Malati, P., Huo, Y.X., Cho, K.M., and Liao, J.C. (2012). Integrated electromicrobial conversion of CO_2 to higher alcohols. Science *335*, 1596.
27. Lee, M.G., Li, X.-Y., Ozden, A., Wicks, J., Ou, P., Li, Y., Dorakhan, R., Lee, J., Park, H.K., Yang, J.W., et al. (2023). Selective synthesis of butane from carbon monoxide using cascade electrolysis and thermocatalysis at ambient conditions. Nat. Catal. *6*, 310–318.
28. Zheng, T., Zhang, M., Wu, L., Guo, S., Liu, X., Zhao, J., Xue, W., Li, J., Liu, C., Li, X., et al. (2022). Upcycling CO_2 into energy-rich long-chain compounds via electrochemical and metabolic engineering. Nat. Catal. *5*, 388–396.
29. Cai, T., Sun, H., Qiao, J., Zhu, L., Zhang, F., Zhang, J., Tang, Z., Wei, X., Yang, J., Yuan, Q., et al. (2021). Cell-free chemoenzymatic starch synthesis from carbon dioxide. Science *373*, 1523–1527.
30. Sheng, H., Janes, A.N., Ross, R.D., Hofstetter, H., Lee, K., Schmidt, J.R., and Jin, S. (2022). Linear paired electrochemical valorization of glycerol enabled by the electro-Fenton process using a stable $NiSe_2$ cathode. Nat. Catal. *5*, 716–725.
31. Li, Y., Ozden, A., Leow, W.R., Ou, P., Huang, J.E., Wang, Y., Bertens, K., Xu, Y., Liu, Y., Roy, C., et al. (2022). Redox-mediated electrosynthesis of ethylene oxide from CO_2 and water. Nat. Catal. *5*, 185–192.
32. Li, R., Xiang, K., Peng, Z., Zou, Y., and Wang, S. (2021). Recent advances on electrolysis for simultaneous generation of valuable chemicals at both anode and cathode. Adv. Energy Mater. *11*, 2102292.
33. Leow, W.R., Lum, Y., Ozden, A., Wang, Y., Nam, D.H., Chen, B., Wicks, J., Zhuang, T.T., Li, F., Sinton, D., et al. (2020). Chloride-mediated selective electrosynthesis of ethylene and propylene oxides at high current density. Science *368*, 1228–1233.
34. Chung, M., Jin, K., Zeng, J.S., and Manthiram, K. (2020). Mechanism of chlorine-mediated electrochemical ethylene oxidation in saline water. ACS Catal. *10*, 14015–14023.
35. Wen, G., Ren, B., Zheng, Y., Li, M., Silva, C., Song, S., Zhang, Z., Dou, H., Zhao, L., Luo, D., et al. (2021). Engineering electrochemical surface for efficient carbon dioxide upgrade. Adv. Energy Mater. *12*, 2103289.

36. Wang, Y., Han, P., Lv, X., Zhang, L., and Zheng, G. (2018). Defect and interface engineering for aqueous electrocatalytic CO_2 reduction. Joule *2*, 2551–2582.

37. Su, C., Shao, Z., Lin, Y., Wu, Y., and Wang, H. (2012). Solid oxide fuel cells with both high voltage and power output by utilizing beneficial interfacial reaction. Phys. Chem. Chem. Phys. *14*, 12173–12181.

38. Lian, T., Koper, M.T.M., Reuter, K., and Subotnik, J.E. (2019). Special topic on interfacial electrochemistry and photo(electro)catalysis. J. Chem. Phys. *150*, 041401.

39. Gordon, C.P., Engler, H., Tragl, A.S., Plodinec, M., Lunkenbein, T., Berkessel, A., Teles, J.H., Parvulescu, A.N., and Copéret, C. (2020). Efficient epoxidation over dinuclear sites in titanium silicalite-1. Nature *586*, 708–713.

40. Lum, Y., Huang, J.E., Wang, Z., Luo, M., Nam, D.-H., Leow, W.R., Chen, B., Wicks, J., Li, Y.C., Wang, Y., et al. (2020). Tuning OH binding energy enables selective electrochemical oxidation of ethylene to ethylene glycol. Nat. Catal. *3*, 14–22.

41. Wang, A., and Zhang, T. (2013). One-pot conversion of cellulose to ethylene glycol with multifunctional tungsten-based catalysts. Acc. Chem. Res. *46*, 1377–1386.

42. Lane, B.S., and Burgess, K. (2003). Metal-catalyzed epoxidations of alkenes with hydrogen peroxide. Chem. Rev. *103*, 2457–2473.

43. Russo, V., Tesser, R., Santacesaria, E., and Di Serio, M. (2013). Chemical and technical aspects of propene oxide production via hydrogen peroxide (HPPO process). Ind. Eng. Chem. Res. *52*, 1168–1178.

44. Guan, M.H., Dong, L.Y., Wu, T., Li, W.C., Hao, G.P., and Lu, A.H. (2023). Boosting Selective Oxidation of ethylene to ethylene glycol Assisted by in situ Generated H_2O_2 from O_2 electroreduction. Angew. Chem. Int. Ed. Engl. *62*, e202302466.

45. Lucky, C., Wang, T., and Schreier, M. (2022). Electrochemical ethylene oxide synthesis from ethanol. ACS Energy Lett. *7*, 1316–1321.

46. Ko, M., Kim, Y., Woo, J., Lee, B., Mehrotra, R., Sharma, P., Kim, J., Hwang, S.W., Jeong, H.Y., Lim, H., et al. (2022). Direct propylene epoxidation with oxygen using a photo-electro-heterogeneous catalytic system. Nat. Catal. *5*, 37–44.

47. Teržan, J., Huš, M., Likozar, B., and Djinović, P. (2020). Propylene epoxidation using molecular oxygen over copper- and silver-based catalysts: a review. ACS Catal. *10*, 13415–13436.

48. Lei, Y., Mehmood, F., Lee, S., Greeley, J., Lee, B., Seifert, S., Winans, R.E., Elam, J.W., Meyer, R.J., Redfern, P.C., et al. (2010). Increased silver activity for direct propylene epoxidation via subnanometer size effects. Science *328*, 224–228.

49. Zhang, X., Zhao, X., Zhu, P., Adler, Z., Wu, Z.-Y., Liu, Y., and Wang, H. (2022). Electrochemical oxygen reduction to hydrogen peroxide at practical rates in strong acidic media. Nat. Commun. *13*, 2880.

50. Xia, Y., Zhao, X., Xia, C., Wu, Z.Y., Zhu, P., Kim, J.Y.T., Bai, X., Gao, G., Hu, Y., Zhong, J., et al. (2021). Highly active and selective oxygen reduction to H_2O_2 on boron-doped carbon for high production rates. Nat. Commun. *12*, 4225.

51. Xia, C., Xia, Y., Zhu, P., Fan, L., and Wang, H. (2019). Direct electrosynthesis of pure aqueous H_2O_2 solutions up to 20% by weight using a solid electrolyte. Science *366*, 226–231.

52. Wang, Q., Wang, L., Chen, J., Wu, Y., and Mi, Z. (2007). Deactivation and regeneration of titanium silicalite catalyst for epoxidation of propylene. Journal of Molecular Catalysis A: Chemical *273*, 73–80.

53. Thiele, G. (1997). Process for the Production of Epoxides from Olefins. Google patent US 5675026.

54. Clerici, M.G., and Ingallina, P. (1993). Epoxidation of lower olefins with hydrogen peroxide and titanium silicalite. J. Catal. *140*, 71–83.